The Electrochemical Properties of Porous Carbon Derived from the Prawn as Anode for Lithium Ion Batteries

Xin Lian[1], Qidong Li[2], Yanming Zhao[1,3,*], Shenghong Liu [1], Huatao Liu[2], Hui Zhang[2]

[1] School of Physics, South China University of Technology, Guangzhou, 510640, China
[2] School of Material Science and Engineering, South China University of Technology, Guangzhou, 510640, P. R. China
[3] State Key Laboratory of Luminescent Materials and Devices, South China University of Technology, Guangzhou, 510640, P. R. China
[*]E-mail: zhaoym@scut.edu.cn

Porous carbon materials derived from the prawn shell (PSC) and prawn meat (PMC) have been successfully fabricated by a simple "curing" method, followed by an annealing process. The PSC and PMC are well characterized by XRD, Raman, SEM and TEM. Electrochemical measurements reveal that PSC and PMC deliver high initial discharge/charge capacities of 1735/878 mAh g^{-1} and 1132/674 mAh g^{-1} at 100 mA g^{-1} and maintain charge capacity retention of 84.2% and 40.3% after 90 cycles, respectively. Moreover, the PSC exhibits a high reversible capacity of 300 mAh g^{-1} after 50 cycles at 1000 mA g^{-1}. The outstanding electrochemical performance of PSC and PMC is attributed to the coherent interconnected porous structure and nitrogen doping, which is beneficial for fast penetration of electrolyte, rapid diffusion of Li$^+$ and creation of numerous active sites for Li$^+$ storage.

1. INTRODUCTION

Lithium ion batteries (LIBs) have been considered as one of the most promising energy storage systems for portable and smart devices (e.g., MP3, cell phones and laptops) and electric vehicles (EVs, including hybrid- and plug-in EVs) [1]. It is believed that suitable electrode materials with high power/energy densities and low cost is a key to success of LIBs for their large-scale applications in EVs [2-4]. Graphite as anode for LIBs has achieved great success mainly due to cycling stability, long cycle life and low cost [5, 6]. However, it suffers from low specific capacity, poor rate capability and risk of the formation of lithium dendrite resulted from its low working potential [7, 8]. To address these critical issues, tremendous efforts have been devoted to searching alternative anodes.

Carbonaceous materials are ideal alternative candidates to graphite. This is mainly due to their high electric conductivity, high specific capacity and excellent chemical stability. Among the carbonaceous materials, activated carbon species derived from the abundant natural bio-precursors, such as cotton wool [9], coffee shells [10], rice husk [11], alginic acid [12], pine cone flowers [13], have drawn much attention over the past years. Such kinds of materials often possess rich porous structures and high specific surface area. In order to obtain high-performance activated carbon, several preparation methods have been developed. The common routes include: (i) the chemical activation of the biomass precursors with the use of strong chemical acid or alkaline reagent, like NaOH [14, 15], KOH [16] and H_3PO_4 [17]; (ii) the physical activation via the steam or CO_2 treatment [18, 19]. However, these common routes often involve the use of strong chemical reagent in the chemical activation process and need multiple or even complex preparation procedures. Therefore, to search simple and effective methods for the preparation of activation carbon from biomass has been attracted great attentions.

Marine biomasses (e.g., prawn, squid and crab) are kinds of natural abundant resource. These biomasses contain rich chitin and protein. Moreover, the activation carbon from such kinds of marine biomass with high level nitrogen content is beneficial for improving lithium storage properties [14, 15]. As aforementioned, searching a simple and effective method for the treatment of marine biomass become critically important. Herein, we have successfully employed a simple "curing" (often used in food process [20]) method to produce high-quality activated carbon from prawn. In the "curing" method, the prawn as raw material was directly placed in the NaCl saturated solution for "curing" treatment. During this process, NaCl evenly infiltrates into the tissue of the prawn, which is favorable for the subsequent formation of rich porous structures. The residual NaCl within the activation carbon that was carbonized from as-prepared shell and meat can be removed easily and completely by using distilled water. For the biomass composed with shell (rich in chitin) and meat (rich in protein), most reports focused on the research of biomass shells because they are often considered as "waste". Although few attentions have been paid to the carbon activated from biomass meat, it is expected that meat may also be a good candidate as anode for LIBs. Here, benefitting from rich porous structures and high nitrogen doping level, activated carbon materials derived from the prawn shell (PSC) and prawn meat (PMC) display good lithium storage properties.

2. EXPERIMENTAL

2.1. Materials synthesis

Firstly, prawn was placed in the saturated NaCl solution at 100 °C for 30 min to destruct the cell membrane activity of the prawn. This process avails the permeation of NaCl into the interior of cell. To promote the deep uptake of NaCl, the prawn was transferred into a beaker with the saturated NaCl solution for 5 days. After that, the resulted prawn was separated into the shell (rich in chitin) and meat (rich in protein) and dried at 80°C in a blast oven. Then, prawn shell and meat were carbonized at 700 °C for 5 h under an atmosphere of H_2/Ar (30/70 vol. %). In order to remove the insoluble metal

ion (i.e., Ca/Ca^{2+}) as well as the soluble ions (e.g., K$^+$, Na$^+$, Cl$^-$), the resulted samples were washed completely with 1 M HCl and deionized water. Finally, the black products from prawn shell (PSC) and prawn meat (PMC) were collected by centrifuging at a speed of 14000 rpm with Allegra X-22 Centrifuge (Beckman Coulter, USA) and dried at 80 °C in vacuo.

2.2. Sample Characterization

Powder X-ray diffraction (XRD) patterns and Raman spectroscopy of the PSC and PMC were performed on a Bruker D8 Advance Diffractometer and LabRAM Aramis, respectively. The morphologies of the PSC and PMC were confirmed by field-emission scanning electron microscopy (FE-SEM, Nova NanoSEM430) and transmission electron microscope (TEM, FEI (Tecnai 20 G2). X-ray photoelectron spectroscopy (XPS) was measured using a Kratos Axis Ultra spectrometer. The centrifugal process was performed on an Allegra X-22 Centrifuge (Beckman Coulter, USA).

2.3. Electrochemical measurements

Electrochemical performance of the PSC and PMC samples was measured in coin-cell using a battery tester system (Land® CT2001A, China). The coin type cells were fabricated in a Mikrouna glove box with ultra-high-purity argon. The electrodes were prepared by mixing the active materials (*i.e.* PSC and PMC), polyvinylidene fluoride (PVDF) and acetylene black (AC) in a weight ratio of 7:1:2. The mixing solvent is N-methyl-2-pyrrolidone. Then, the resulted slurry was uniformly coated on Cu foil and then placed in a vacuum oven at 80°C overnight. The mass loading on the electrode was ~ 2 mg cm^{-2}. The coin-cells were fabricated by lithium metal foil as the counter electrode, Celgard 2320 as separator, the resulted electrode as working electrode and 1 M LiPF$_6$ in ethylene carbonate (EC): dimethyl carbonate (DMC) 1:1 (vol.%) as the electrolyte. Electrochemical impedance spectroscopy (EIS) was performed on an AUTOLAB PGSTAT302N (Metrohm, Netherlands).

3. RESULTS AND DISCUSSIONS

The X-ray diffraction (XRD) patterns of PSC and PMC are shown in Fig. 1a, where two broad diffraction peaks around 24° and 43° for both PSC and PMC samples are corresponding to characteristic peaks of (002) and (100) of amorphous carbon, respectively. The interlayer d-spacing of about 0.364 nm for (002) of PSC and PMC is higher than that for graphite (0.335 nm), which should be beneficial for lithium ions transportation. Fig. 1b shows Raman spectra of PSC and PMC. As shown in Fig. 1b, two characteristic peaks of carbon centered at 1340 cm^{-1} (D band) and 1590 cm^{-1} (G band) can be observed. The D band and G band are associated with the defective and disordered structures and the in-plane vibrations of carbon atoms with sp^2 electronic configuration in graphitic phase respectively [21, 22]. The intensity ratio of I$_D$/I$_G$ for PSC (0.99) is higher than that for PMC (0.85), indicating that more defects existing in PSC.
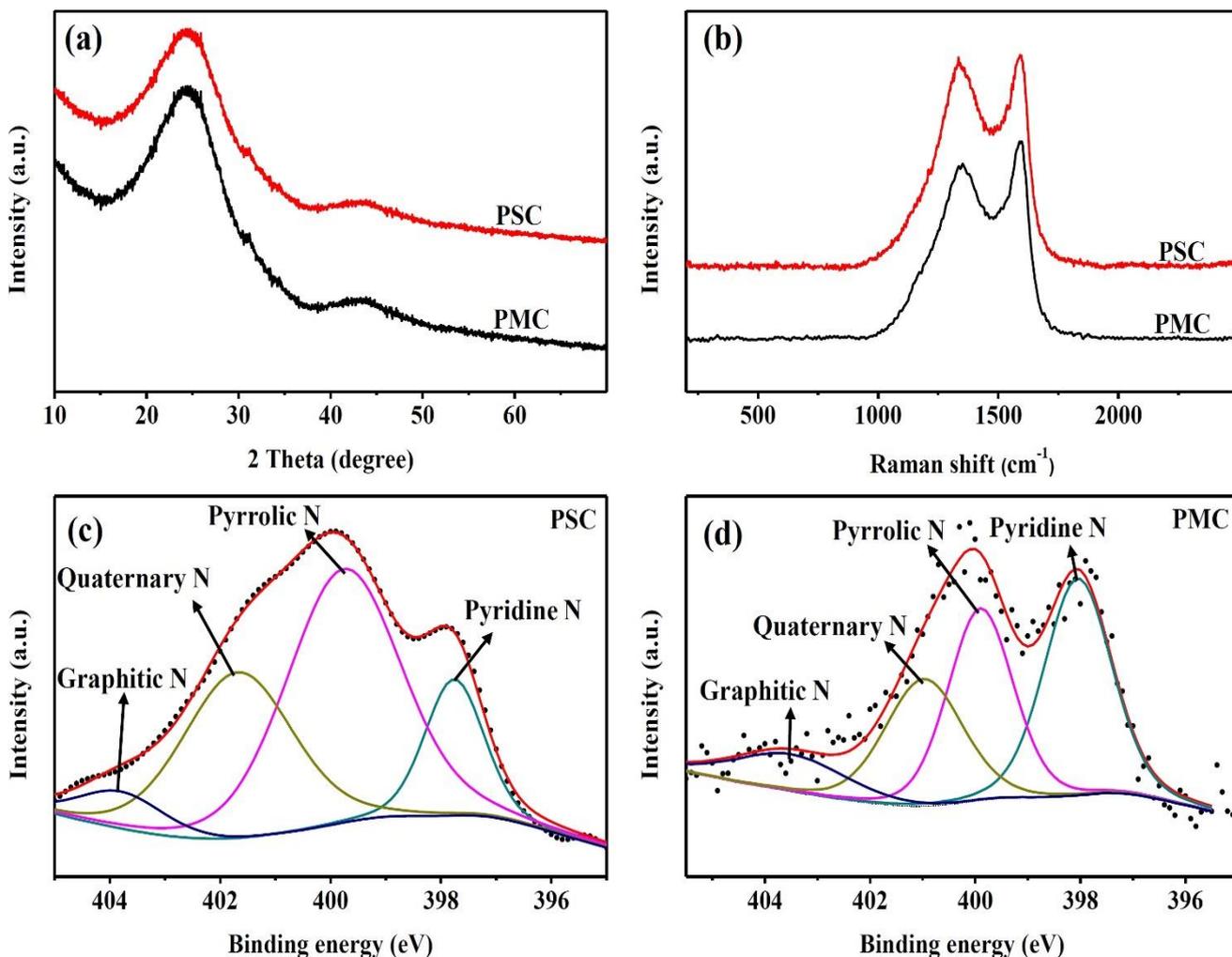
Figure 1. (a) XRD patterns and (b) Raman spectra of PSC and PMC, and high resolution XPS N 1s peak of (c) PSC and (d) PMC.

It is well known that nitrogen doping to carbon (N-C) could lead N-C with the enhanced lithium ion storage properties [23, 24]. This is mainly due to the higher electronegativity of nitrogen than that of carbon, and additional active sites for lithium ions storage. In order to identify the nitrogen states of PSC and PMC, XPS of PSC and PMC was carried out as shown in Fig. 1c-d. As can be seen, the nitrogen peaks for PSC and PMC can be further convoluted into graphitic N (403.8 ± 0.2 eV), quaternary N (400.8 ± 0.2 eV), pyrrolic N (399.7 ± 0.2 eV) and pyridinic N (398.0 ± 0.2 eV). This result is consistent with the previous reported data [17, 25].

The SEM and TEM images of PSC and PMC shown in Fig. 2 illustrate that both PSC and PMC have porous structures (Fig. 2a-b). PSC has smaller and much uniform pores with a diameter of ~ 50 nm (Fig. 2c) if one compare it with that of PMC. Generally, the 3D porous network can provide quick penetration of electrolyte and fast diffusion of lithium ions, and large surface area for lithium ions storage. Furthermore, the detailed structural information of PSC was further confirmed by HRTEM and SAED. As shown in Fig. 2d, the PSC shows the amorphous pattern, which agrees well with the XRD results.
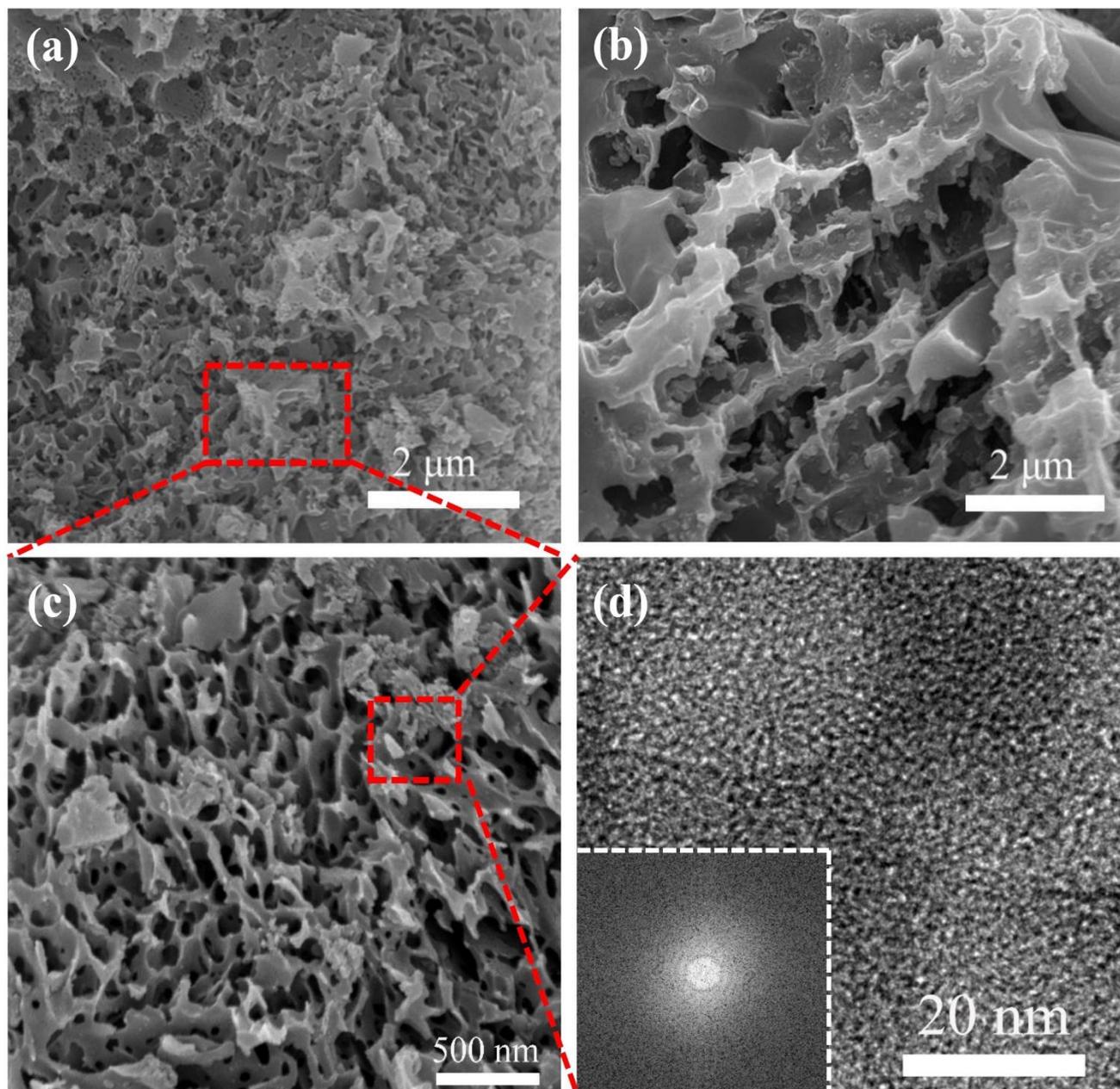
Figure 2. SEM images of (a, c) PSC and (b) PMC. (d) HRTEM image of PSC. Inset of Fig. 2d: Selected area electron diffraction (SAED).

The discharge-charge curves of PSC and PMC (Fig. 3a-b) for initial 3 cycles at 30 mA g^{-1} in the voltage between 0.005 and 3.0 V agree well with typical carbonaceous materials as anodes for LIBs [23-25]. As shown in Fig.3a, the PSC and PMC exhibit high initial discharge/charge capacities of 1803/910 mAh g^{-1} and 1200/694 mAh g^{-1}, corresponding to initial Coulombic efficiencies (CEs) of 50.4% and 57.8%, respectively. The formation of solid electrolyte interface (SEI) on the surface of PSC and PMC should be a key role for the relatively low initial CE [26]. After the first cycle, the Coulombic efficiencies increased quickly to 91.0% (PSC) and 92.7% (PMC) for the second cycle, 93.7% (PSC) and 94.5% (PMC) for the third cycle, and eventually to hover nearly 100% afterward. As shown in the insets of Fig. 3a-b, the results from electrochemical voltage spectroscopy (EVS)

differential capacity curves of PSC and PMC for the first three cycles are almost consistent with the corresponding discharge-charge profiles (Fig. 3a-b). It should be noted that, there was a distinct oxidation peak centered at ~1.1 V (Fig. 3a), most likely corresponding to delithiation process of Li-oxygen containing functional groups. The highly overlapped peaks during the following cycles further indicate good reversibility of PSC and PMC (especially for PSC).
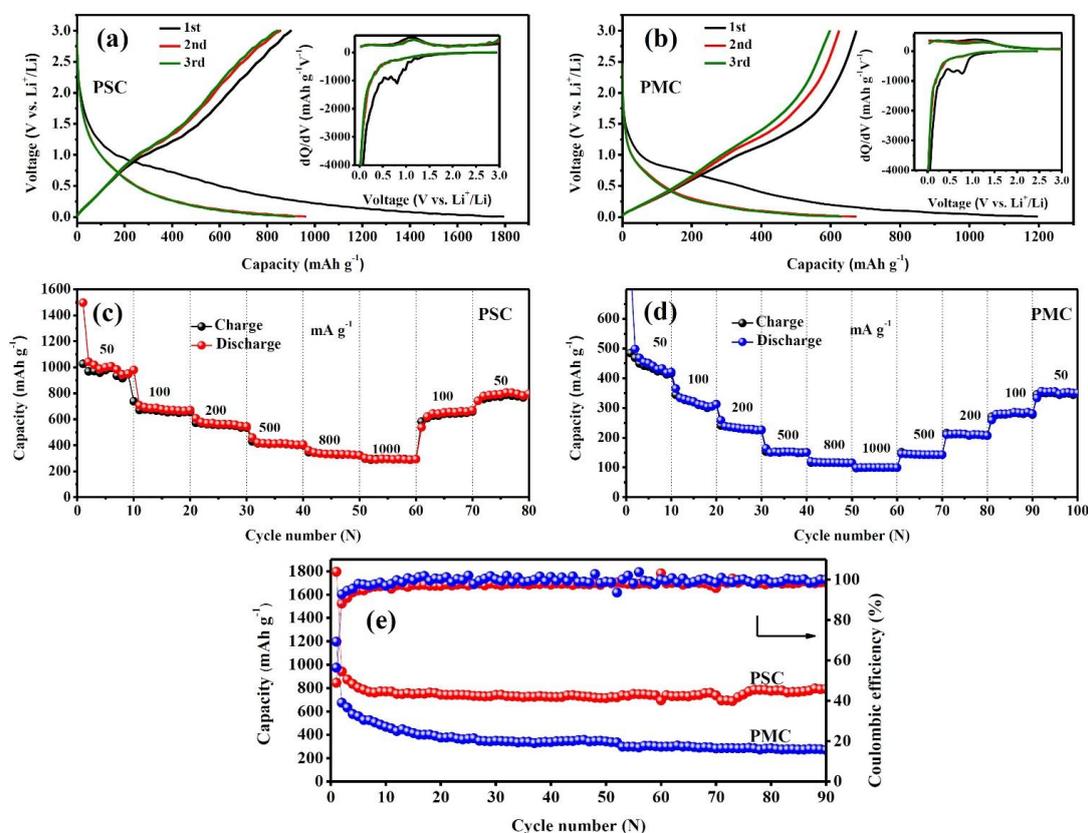

Figure 3. Discharge-charge curves of (a) PSC and (b) PMC for initial three cycles at 30 mA g^{-1}, rate capability of (c) PSC and (d) PMC at different current densities; and (e) cycling performance of PSC and PMC at 100 mA g^{-1}. Insets of Fig. 3a-b are the corresponding EVS differential capacity data.

The rate capabilities of PSC and PMC are evaluated at various current densities ranging from 50 to 1000 mA g^{-1} between 0.005 and 3.0 V (Fig. 3c-d). As the current densities increased from 50 to 1000 mA g^{-1}, the PSC shows excellent rate capability with high average reversible capacities of 950, 674, 572, 430, 347 and 300 mAh g^{-1} at 50,100, 200, 500, 800 and 1000 mA g^{-1}, respectively, which are higher than those for PMC (420, 345, 241, 153, 117 and 100 mAh g^{-1}). This can be attributed to more rich and uniform nanoporous structures of PSC than that of PMC, as well as its higher nitrogen doping level. Since the current density is set back to 50 mA g^{-1}, the PSC and PMC still demonstrate excellent reversibility and recoverability. Fig. 3e shows the cycling performance of the PSC and PMC at 100 mA g^{-1} for 90 cycles. As can be seen, the PSC exhibits more excellent stability with the reversible capacity retention of ~ 84.2% (PSC) after 90 cycles, which is higher than that for PMC (40.3%).

Table 1. Comparison of the carbon derived from biomass for lithium ion batteries with previous reported studies.

Biomass precursor	Activation method	Temperature (℃)	Capacity (mAh g^{-1})	Ref.
Prawn shell (I) Prawn meat	NaCl	700	950 at 0.05 A g^{-1}, 300 at 1 A g^{-1} 420 at 0.05A g^{-1}, 100 at 1A g^{-1}	This work
Cotton wool	One step pyrolysis Multi step pyrolysis	700-1100	470 600	[9]
Coffee shells	Untreated KOH-treated	800,900 800,900	524,603 at 0.2 C of the 1st discharge 1150,1200 at 0.2 C of the 1st discharge	[10]
Rice husk	Hydrothermal carbonization	180-250	403 at 0.2 C (100 cycles) 137 at 10 C	[11]
Prawn shell (II)	NaOH-treated	750	740 at 0.1 A g^{-1} (150 cycles) 147 at 2 A g^{-1}	[14]
Ox horns	KOH-treated	700	1181 at 0.1 A g^{-1} 304 at 5 A g^{-1}	[16]
Rice straw	KOH-treated	800	986 of the 1st cycle at 0.1 C 257 at 2 C	[27]
Fish scale	KOH-treated	850	500 at 0.075 A g^{-1} 450 at 0.2 A g^{-1}	[28]
Wheat straw	KOH activation	700	975 at 0.37 A g^{-1} 731 at 1.85 A g^{-1} 664 at 3.7 A g^{-1}	[29]
Human hair (I)	KOH-treated	800	700 at 0.05 A g^{-1} 610 at 0.1 A g^{-1}	[30]
Human hair (II)	HCl pretreatment, KOH activation	700	1331 at 0.1 A g^{-1} 470 at 5 A g^{-1} 205 at 10 A g^{-1}	[31]
Egg white (I)	Untreated	600	580 at 0.005 A g^{-1}	[32]
Egg white (II)	Templating method	650-850	1780 of the 2nd cycle at 0.1 A g^{-1} 205 at 4 A g^{-1}	[33]
Honey	Templating method	700-900	1359 at 0.1 A g^{-1} (after 10 cycles) 722 at 1 A g^{-1} (after 200 cycles) 390 at 5 A g^{-1}	[34]
Gelatin	Templating method	700-900	1200 at 0.1 mA cm^{-1} 400 at 0.8 mA cm^{-1}	[35]

The comparison of the carbon derived from biomass for lithium ion batteries with previous reported studies is included in Table 1, where the PSC and PMC fabricated by a facile "curing" method here exhibit comparative high electrochemical performance. Without involving the strong chemical reagent (*e.g.* KOH and NaOH) [10, 14, 16, 27-31] during the synthesis route as well as avoiding the tedious preparation procedures in the templating method [33-35], the "curing" method adopted here will present a simple and cost-effective method for the preparation of activation carbon from other biomass.
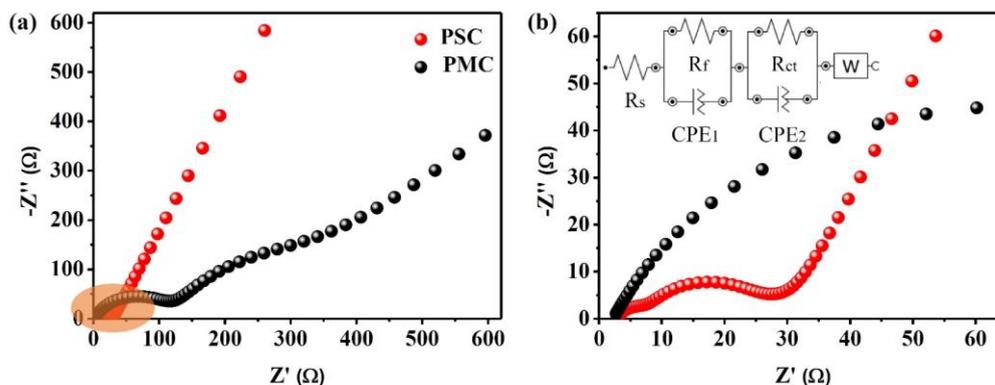
Figure 4. (a, b) EIS plots of PSC and PMC measured after 3 cycles. Inset of Fig. 4b: the equivalent circuit model for EIS analysis.

In order to understand the transport kinetics of the PSC and PMC electrodes, EIS measurements are shown in Figure 4. After three discharge-charge cycles and then rest for 3 hours, the cells were measured at 100 mA g^{-1} in the voltage range of 0.005-3 V. As shown in Fig. 4a-b, the PSC and PMC cells show typical Nyquist plots consisting of two depressed semicircles in the high- and medium-frequency regions and a sloping straight line in the low-frequency region. The equivalent circuit model was fabricated in the inset of Fig. 4b. The fabricated model includes internal resistance (R_s) in the high- and medium-frequency region, two constant phase element (CPE_1, CPE_2), SEI resistance R_f, charge transfer resistance (R_{ct}) in the medium/low frequency region, and Warburg impedance (W) in the unclear ~45° inclined line in the low-frequency region. The R_{ct} is a key indicator of charge-transfer kinetics, which is approximately equal to the numerical value of the 2nd semicircle. As a result, the PSC shows the lower charge transfer resistance (~ 16Ω) than PMC (~ 120Ω), which is consistent with electrochemical performance.

4. CONCLUSIONS

Amorphous and porous carbon derived from the prawn shell (PSC) and prawn meat (PMC) have been successfully fabricated by a simple "curing" method, followed by an annealing process. Benefitting from the rich porous structures and high nitrogen doping content, the PSC and PMC deliver high initial discharge/charge capacities of 1735/878 mAh g^{-1} and 1132/674 mAh g^{-1} at 100 mA g^{-1} and retain the charge capacity retention of 84.2% and 40.3% after 90 cycles, respectively. Moreover, the PSC exhibits a high discharge capacity of 300 mAh g^{-1} after 50 cycles at 1000 mA g^{-1}. The excellent electrochemical performance of porous carbonaceous materials derived from the prawn (especially PSC) is attributed to the coherent interconnected porous structure that effectively make it for quick penetration of electrolyte, rapid diffusion of Li^+ and numerous active sites for Li^+ storage.

References

1. M. Armand, J.M. Tarascon, *Nature*, 451 (2008) 652.
2. J.B. Goodenough, Y. Kim, *Chem. Mater.*, 22 (2009) 587.
3. J. Xu, S. Dou, H. Liu, L. Dai, *Nano Energy*, 2 (2013) 439.
4. C. Liang, M. Gao, H. Pan, Y. Liu, M. Yan, *J. Alloys Compd.*, 575 (2013) 246.
5. T. Tran, J. Feikert, X. Song, K. Kinoshita, *J. Electrochem. Soc.*, 142 (1995) 3297.
6. S. Yang, X. Feng, L. Zhi, Q. Cao, J. Maier, K. Müllen, *Adv. Mater.*, 22 (2010) 838.
7. S.S. Zhang, *J. Power Sources*, 161 (2006) 1385.
8. B. Simon, S. Flandrois, K. Guerin, A. Fevrier-Bouvier, I. Teulat, P. Biensan, *J. Power Sources*, 81 (1999) 312.
9. E. Peled, V. Eshkenazi, Y. Rosenberg, *J. Power Sources*, 76 (1998) 153.
10. Y.J. Hwang, S.K. Jeong, K.S. Nahm, J.S. Shin, A.M. Stephan, *J. Phys. Chem. Solids*, 68 (2007) 182.
11. L. Wang, Z. Schnepp, M.M. Titirici, *J. Mater. Chem. A*, 1 (2013) 5269.
12. X.L. Wu, L.L. Chen, S. Xin, Y.X. Yin, Y.G. Guo, Q.S. Kong, Y.Z. Xia, *Chemsuschem*, 3 (2010) 703.
13. G. Nagaraju, J.H. Lim, S.M. Cha, J.S. Yu, *J. Alloys Compd.*, 693 (2017) 129.
14. I. Elizabeth, B.P. Singh, S. Trikha, S. Gopukumar, *J. Power Sources*, 329 (2016) 412.
15. F. Gao, J. Qu, Z. Zhao, Z. Wang, J. Qiu, *Electrochim. Acta*, 190 (2016) 1134.
16. J. Ou, Y. Zhang, L. Chen, Q. Zhao, Y. Meng, Y. Guo, D. Xiao, *J. Mater. Chem. A*, 3 (2015) 6534.
17. J. Qu, C. Geng, S. Lv, G. Shao, S. Ma, M. Wu, *Electrochim. Acta*, 176 (2015) 982.
18. F. Rodriguez-Reinoso, M. Molina-Sabio, M. Gonzalez, *Carbon*, 33 (1995) 15.
19. T. Zhang, W.P. Walawender, L. Fan, M. Fan, D. Daugaard, R. Brown, *Chem. Eng. J.*, 105 (2004) 53.
20. I. Siró, C. Vén, C. Balla, G. Jónás, I. Zeke, L. Friedrich, *J. Food. Eng.*, 91 (2009) 353.
21. J. Xu, I.Y. Jeon, J.M. Seo, S. Dou, L. Dai, J.B. Baek, *Adv. Mater.*, 26 (2014) 7317.
22. W. Guo, X. Li, J. Xu, H.K. Liu, J. Ma, S.X. Dou, *Electrochim. Acta*, 188 (2016) 414.
23. J. Xu, Y. Lin, J.W. Connell, L. Dai, *Small*, 11 (2015) 6179.
24. J. Xu, J. Mahmood, Y. Dou, S. Dou, F. Li, L. Dai, J.B. Baek, *Adv. Mater.*, 29 (2017).
25. Z. Li, Z. Xu, X. Tan, H. Wang, C.M. Holt, T. Stephenson, B.C. Olsen, D. Mitlin, *Energy Environ. Sci.*, 6 (2013) 871.
26. M. Winter, J.O. Besenhard, M.E. Spahr, P. Novák, *Adv. Mater.*, 10 (1998) 725.
27. F. Zhang, K. Wang, G. Li, J. Chen, *Electrochem. Commun.*, 11 (2009) 130.
28. V. Selvamani, R. Ravikumar, V. Suryanarayanan, D. Velayutham, S. Gopukumar, *Electrochim. Acta*, 182 (2015) 1.
29. L. Chen, Y. Zhang, C. Lin, W. Yang, Y. Meng, Y. Guo, M. Li, D. Xiao, *J. Mater. Chem. A*, 2 (2014) 9684.
30. K. Saravanan, N. Kalaiselvi, *Carbon*, 81 (2015) 43.
31. J. Ou, Y. Zhang, L. Chen, H. Yuan, D. Xiao, *Rsc Adv.*, 4 (2014) 63784.
32. X. Liu, M. Wen, Y. Zhao, Y. Dong, Q. Fan, Q. Kuang, Q. Li, *Rsc Adv.*, 6 (2016) 80986.
33. Z. Li, Z. Xu, X. Tan, H. Wang, C.M. Holt, T. Stephenson, B.C. Olsen, D. Mitlin, *Energy Environ. Sci.*, 6 (2013) 871.
34. Y. Zhang, L. Chen, Y. Meng, J. Xie, Y. Guo, D. Xiao, *J. Power Sources*, 335 (2016) 20.
35. Y. Mao, H. Duan, B. Xu, L. Zhang, Y. Hu, C. Zhao, Z. Wang, L. Chen, Y. Yang, *Energy Environ. Sci.*, 5 (2012) 7950.